Fiber-Specific Electrostriction Response Under Intensity Modulation

Fatima Al-Shaikhli, Maurice O'Sullivan and Rongqing Hui

Abstract—Electrostriction in an optical fiber is introduced by interaction between the forward propagated optical signal and the acoustic standing waves in the radial direction resonating between the center of the core and the cladding circumference of the fiber. The response of electrostriction is dependent on fiber parameters, especially the mode field radius. We demonstrated a novel technique that can be used to characterize fiber properties by means of measuring their electrostriction response under intensity modulation. As the spectral envelope of electrostriction-induced propagation loss is anti-symmetrical, the signal to noise ratio can be significantly increased by subtracting the measured spectrum from its complex conjugate. We show that if the transversal field distribution of the fiber propagation mode is Gaussian, the envelope of the electrostriction-induced loss spectrum closely follows a Maxwellian distribution whose shape can be specified by a single parameter determined by the mode field radius.

Index Terms— optical fiber, optical fiber measurement, optical fiber communication, optical fiber nonlinearity

I. INTRODUCTION

An optical signal traveling in an optical fiber can create acoustic waves propagating in both longitudinal and radial directions. The interaction between the optical signal and the longitudinal sound wave is known to cause optical backscattering in a process commonly referred to as stimulated Brillouin scattering (SBS) [1], which is equivalent to a nonlinear loss. Whereas the acoustic wave propagating in the radial direction is bounced back and forth between the center and circumference of the cladding/coating interface [2, 3] to create acoustic standing waves that modulate the effective refractive index of the fiber. This results in a complex modulation of the forward propagated optical signal in the frequency region typically below 2 GHz depending on the fiber type. This effect is commonly known as electrostriction. The complex response of electrostriction in a single-mode fiber is determined by the mechanical properties of silica material, the geometry of the optical fiber, and the mode field radius. This provides a mechanism for characterizing fiber properties through measuring the complex frequency response of electrostriction. In practical optical networks, different types of optical fibers may coexist, and simple techniques to identify fiber types are desirable for network operation and performance optimization.

Measurements of frequency-dependent electrostriction in optical fibers have been reported, primarily using cross-phase modulation (XPM) in pump-probe configurations. In such measurements, phase modulation on the continuous-wave (CW) probe introduced by an intensity-modulated pump is measured to determine the real part of the frequency-dependent nonlinear refractive index of electrostriction, n_{2e} [4 – 6]. Selfphase modulation (SPM) can also be used to characterize n_{2e} by measuring the complex optical field change of an intensity modulated optical signal traveling through a fiber. It is important to note that n_{2e} is complex. While SPM commonly refers to a nonlinear phase modulation which is determined by the real part of n_{2e} , the imaginary part of n_{2e} results in a frequency-dependent gain/loss.

Compared to the XPM technique which requires at least two optical carriers, a single-carrier-based measurement is much simpler, which only requires an intensity modulation bandwidth of less than 3 GHz on the optical carrier to probe the electrostriction response. However, at the receiver it is usually very challenging to separate the very weak intensity perturbation caused by electrostriction from the applied large signal modulation, four-wave mixing (FWM) among different frequency components, system noise, and transmitter/receiver nonlinearities.

In this paper, we demonstrate a simple technique to characterize fiber properties through electrostriction effect based on a single optical carrier. An optical signal is intensitymodulated by a linearly frequency chirped waveform to avoid the impact of intra-channel FWM. Instead of measuring the nonlinear phase change caused by SPM, the frequencydependent loss of the optical carrier which is related to the imaginary part of n_{2e} is measured. Taking advantage of the spectral anti-symmetry of the imaginary part of n_{2e} [2, 6], the impact of electrostriction can be selected by subtracting the coherently detected field from its complex conjugate. We show that if the field distribution of the fiber propagation mode is Gaussian, the envelope of frequency-dependent resonance loss induced by electrostriction closely follows a peak-normalized Maxwellian distribution. This helps fiber type identification using a single parameter. However, if the field distribution of the fiber propagation mode is not Gaussian, such as in a LEAF fiber [7, 8], the envelope of frequency-dependent loss spectrum can deviate from Maxwellian distribution. We use a measure of this deviation to increase the distinguishability of fiber types.

This work was supported in part by the US National Science Foundation under Grant CNS-1956137.

Fatima Al-Shaikhli (fatima.al-shaikhli@ku.edu) and Rongqing Hui (e-mail: rhui@ku.edu) are with the Department of Electrical Engineering and Computer

Science, University of Kansas, Lawrence, KS 66045 USA. Maurice O'Sullivan (mosulliv@ciena.com) is with Ciena Corporation, Ottawa, ON, K2K 0L1, Canada.

Many techniques have been developed over the years to identify fiber types based on fiber attenuation, chromatic dispersion, and nonlinearity [9]. Techniques of characterizing mode field radius relying on nonlinear effects always require absolute calibration of the launched optical power into the fiber. For example, SBS threshold difference of two connected fiber sections can be precisely measured to estimate their mode field radius difference [10], but measuring absolute values of mode field radius is more challenging. The technique presented in this paper based on electrostriction provides an alternative way to characterize fiber properties but without the need to calibrate the signal optical power, and the results are insensitive to chromatic dispersion. In practical applications, this technique can be combined with other techniques to measure additional parameters such as fiber attenuation and chromatic dispersion.

II. THEORETICAL BACKGROUND

The calculation of electrostriction induced nonlinear index change is based on [2, 3]:

$$n_{2e}(t) = U \sum_{m=1}^{\infty} B_m C_m e^{-\Gamma t} \frac{\sin(\Omega_m t)}{\Omega_m} \theta(t)$$
 (1)

Where,

$$B_{m} = -\frac{8\pi}{a^{2}} \int_{0}^{R} \int_{0}^{2\pi} F_{m}(r) \left[\left(\frac{\partial^{2}}{\partial r^{2}} + \frac{1}{r} \frac{\partial}{\partial r} \right) E^{2}(r) \right] r d\varphi dr \qquad (2)$$

$$C_{m} = 2\pi \int_{0}^{R} F_{m}(r) E^{2}(r) r dr$$
(3)

the proportionality coefficient U is determined by a number of material properties of the fiber core, cladding and the nature of cladding/coating interface, and

$$\theta(t) = \begin{cases} 0 & t < 0 \\ 1 & t > 0 \end{cases}$$

 $F_m(r) = M_m J_0(\mu_m r/R)$ is the radial acoustic wave eigenfunction, in which the eigenvalue μ_m can be obtained by solving:

$$[1 - (v_s / v)^2] J_0(\mu_m) - (v_s / v_d)^2 J_2(\mu_m) = 0$$
 (4)

and the normalization factor M_m can be found with,

$$M_{m} = \frac{1}{R\sqrt{\pi[J_{0}^{2}(\mu_{m}) + J_{1}^{2}(\mu_{m})]}}$$
 (5)

where, v_d and v_s are longitudinal and shear sound velocities. J_0 , J_1 , and J_2 are the 0th, 1st and 2nd order Bessel functions, respectively. R is the cladding radius of the fiber. The frequency of the m^{th} acoustic mode is $\Omega_m = \mu_m v_d / R$ and Γ is the damping rate.

For most single mode fibers, mode field in the transversal direction can be approximated by a Gaussian distribution,

$$E(r) = \exp\left(-r^2 / a^2\right) \tag{6}$$

Where a is the mode field radius, and the normalized power density on fiber cross section is $E^2(r) = \exp(-2r^2/a^2)$, so that at r = a the power density is reduced to $1/e^2$ compared to that

at the center of the core. Note that if the radial distribution of field is defined as $E(r) = \exp(-r^2/2a^2)$ as in previous papers [2, 3] including ours [6, 11], the mode field radius would be $\sqrt{2}a$.

Fig.1(a) shows an example of $n_{2e}(t)$ calculated from Eq. (1) using the following parameters: $v_s = 3740$ m/s, $v_d = 5970$ m/s, $\Gamma = 2.5 \times 10^7$ s⁻¹, R = 62.5 µm, and a = 4.91 µm. This represents the impulse response of electrostriction, which includes multiple reflections of soundwave between the center of the fiber core and circumference of the cladding with a roundtrip time $T_{rt} = 2R/v_d \approx 20.94ns$ (corresponding to the time separation between adjacent pulses in Fig.1(a)).

The time-domain impulse response $n_{2e}(t)$ can be converted into $\tilde{n}_{2e}(\Omega)$ in the frequency domain through a Fourier transform. Fig. 1(b) and (c) show the real and the imaginary parts of $\tilde{n}_{2e}(\Omega)$, respectively, each normalized to its maximum value. Sharp resonance spectral lines in $\tilde{n}_{2e}(\Omega)$ are the results of multiple soundwave reflections between the center of the fiber core and circumference of the cladding, and the spacing between adjacent spectral lines is on the order of 48 MHz determined by $1/T_{rt}$. The real part of $\tilde{n}_{2e}(\Omega)$ introduces a frequency-dependent phase change, whereas the imaginary part of $\tilde{n}_{2e}(\Omega)$ represents a frequency-dependent gain or loss of the optical signal.

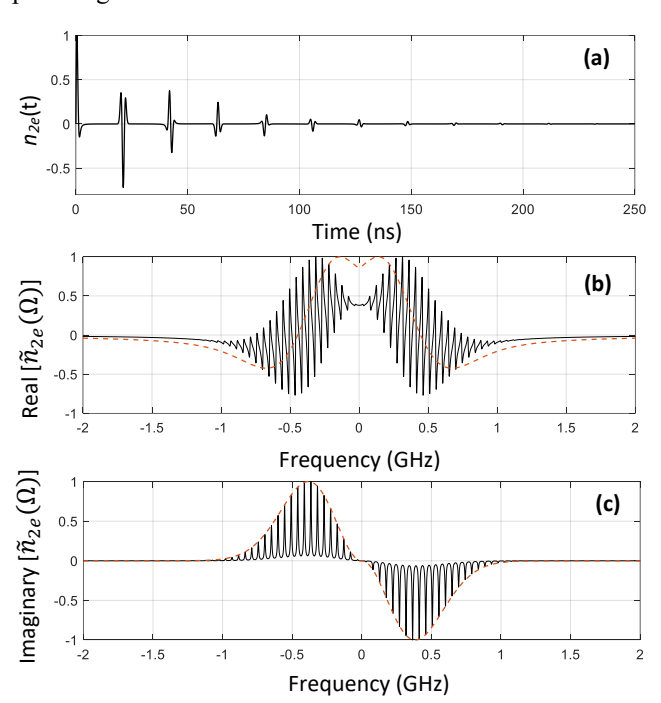


Figure 1 (a): Time domain impulse response of normalized $n_{2e}(t)$. (b) and (c): real and imaginary parts of normalized $n_{2e}(\Omega)$ in the frequency domain.

The dashed lines in Fig.1 (b) and (c) show the envelope of the electrostriction spectrum, $\tilde{n}_{2e,env}(\Omega)$, after removing reflection features from the impulse response. They were calculated from Fourier transform of $n_{2e}(t)$ after forcing $n_{2e}(t)=0$ for t>15ns. This is equivalent to a fiber with an infinite cladding radius, $R\to\infty$. In fact, if the mode field

distribution is Gaussian as described by Eq. (6), the spectral envelope can be expressed as [12],

$$\tilde{n}_{2e,env}(\Omega) = \eta \int_{0}^{\infty} \frac{k^{3} \exp(-k^{2} a^{2} / 4)}{\Omega^{2} - v_{d}^{2} k^{2} - 2j\Gamma\Omega} dk$$
 (7)

Where η is a proportionality factor, Ω is the acoustic angular frequency, v_d is shear sound velocity, and $\Gamma = Ak^2$ is the damping factor with A the coefficient of viscous attenuation and k the acoustic wave number.

Measurement of n_{2e} can be quite challenging because the impact of n_{2e} on signal optical field through electrostriction is weak. The majority of electrostriction characterization techniques are based on pump-probe configurations to measure frequency-dependent phase change of the CW probing optical carrier caused by electrostriction through XPM [4-6]. The measurement of frequency-dependent loss/gain of a single intensity-modulated optical signal can greatly simplify the measurement of electrostriction by eliminating the CW probe. A single-carrier measurement also avoids a potential complication that could be caused by state of polarization (SOP) walk-off between the pump and the probe waves along the fiber. However, because $\tilde{n}_{2e}(\Omega)$ is a very weak perturbation on the optical signal, frequency-dependent gain/loss introduced by electrostriction can be overwhelmed by intensity noise and modulation nonlinearity of the optical signal.

It is important to notice that the imaginary part of $\tilde{n}_{2e}(\Omega)$ shown in Fig. 1(c), which is responsible for the frequency-dependent loss/gain, is anti-symmetrical with respect to the zero frequency. This can be utilized to improve the measurement signal-to-noise ratio (SNR) by subtracting the spectrum from its complex conjugate so that intensity noise, which usually has symmetrical spectrum, can be suppressed.

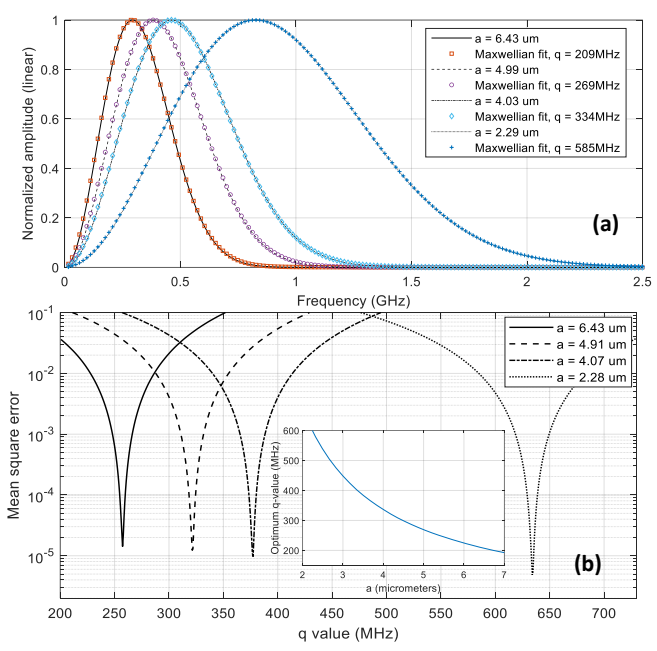


Figure 2. (a) spectral envelopes of $\text{Im}[\tilde{n}_{2e,env}(\Omega)]$ for fibers with different mode field radii, and Maxwellian fitting with optimum q values. (b) Normalized mean square errors of Maxwellian fitting for the 4 fiber types as the function of q-values. Inset in (b): optimum q-value as the function of mode field radius q.

There are various types of single-mode fibers developed over the last few decades and installed in optical communication networks worldwide. Almost all these fibers have very similar cladding diameter of $2R = 125 \pm 1 \, \mu m$, standardized by the International Telecommunications Union (ITU). Thus, the frequency separation between eigen modes does not change significantly for different types of fibers. The most important parameter that can be used to differentiate fiber types is the mode field radius a, or equivalently the effective core area A_{eff} . Therefore, different fiber types can be identified by the loss/gain spectral envelope shown as the dashed line in Fig. 1(c).

To demonstrate the importance of mode field radius on the envelope of electrostriction-induced loss spectrum, Fig. 2(a) shows the normalized spectral envelope of the imaginary part of $\tilde{n}_{2e,env}(\Omega)$ calculated from Eq.(7), for 4 different fiber mode field radii at 1500nm wavelength, $a = 6.43 \,\mu\text{m}$, 4.99 μm , 4.03 µm, and 2.29 µm, corresponding to OFS TeraWave® (G.654.E), Corning SMF-28® (G.652.D), OFS TrueWave-RS®, (G.655) and OFS HSDK®[13] dispersion compensating fiber (DCF), respectively. Other parameters used in the calculation include $v_d = 5970$ m/s and $\Gamma = 2.5 \times 10^7$ s⁻¹. For fibers with smaller core sizes and stronger field concentration near the center of the core, the time domain impulse response of electrostriction is faster, and the spectrum tends to be broader. The envelope of electrostriction-induced loss spectrum of each fiber type shown as solid line in Fig. 2(a) can be fitted closely to a Maxwellian distribution, shown as open dots, with a unique

$$\operatorname{Im}\left\{\tilde{n}_{2e,env}\left(f\right)\right\} = \xi \frac{f^2}{q^3} \exp\left(-\frac{f^2}{2q^2}\right) \tag{8}$$

Where $f = \Omega/2\pi$ is the circular frequency, and ξ is a normalization parameter such that the maximum amplitude is unity. As q is a single parameter that uniquely determines the shape of a Maxwellian distribution, the best fit between the envelope of measured electrostriction spectral envelope and Maxwellian distribution yields an optimum q-value for each fiber type. Fig. 2(b) shows the normalized mean-square-error (MSE) between the imaginary part of $\tilde{n}_{2e}(\Omega)$ calculated from Eq. (7) and Maxwellian distribution with q value as the variable for the 4 fiber types considered in Fig. 2(a). The q values corresponding to the minimum MSE indicate the optimum q values of Maxwellian fits, which are 209 MHz, 269 MHz, 334 MHz, and 585 MHz, respectively for the 4 fiber types. The minimum MSE values for the 4 fiber types are all around 10⁻⁵ in the numerical fitting, which indicates that Maxwellian fitting is appropriate. Inset in Fig. 2(b) shows the monotonic relationship between the q-value and the mode field radius a. A sensitivity function can be found to be $(dq/q)/(da/a) \approx$ -1.05 within the region of $2\mu m < a < 7\mu m$. It needs to be clarified that to obtain Eq. (7), a Gaussian field distribution [Eq. (6)] was assumed. If the mode field distribution is not Gaussian, such as in fibers with refractive index profile (RIP) tailoring, minimum MSE can be used to measure the departure of the envelope of the electrostriction induced loss spectrum from a Maxwellian (to be discussed later).

III. EXPERIMENTAL SETUP, RESULTS AND DISCUSSION

Fig. 3(a) shows the experimental setup, where a tunable laser at 1550 nm wavelength window is used as the light source. The optical carrier is amplitude modulated by an electrooptic intensity modulator before launching into an optical fiber under test. A linearly chirped modulation waveform is generated by an arbitrary wave generator (AWG) as illustrated in the left inset of Fig. 3(b) at 25 GS/s sampling rate. The modulation frequency linearly increases from 25 MHz to 2 GHz within 50 µs as illustrated in the right inset of Fig. 3(b), and the waveform has 1.25 million data points. The time domain waveform is apodized with a 20th order super-Gaussian filter to minimize the edge effect, and the spectrum is shown in Fig. 3(b).

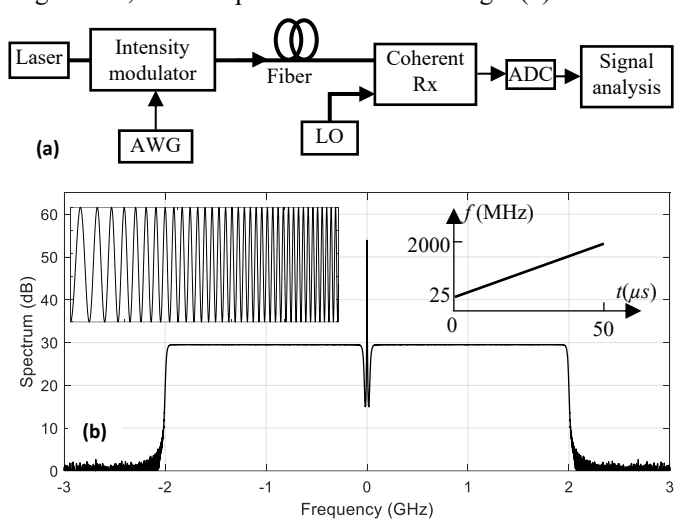


Figure 3. (a): Experimental setup. AWG: arbitrary waveform generator, LO: local oscillator, ADC: analog to digital converter. (b) power spectrum of linearly frequency-chirped waveform with 2 GHz chirping bandwidth. Left-inset: illustration of chirped time domain waveform. Right-inset: time-frequency diagram of linear frequency chirp.

Coherent heterodyne detection is used at the receiver, and the heterodyne electrical signal $E_{het}(t)$ is digitized by a real-time digital analyzer at 25 GS/s sampling speed. In the experiment, we have recorded 10 million data points for analysis, which consists of 8 frames of the chirped waveform. The intensity modulator is biased at the quadrature point to allow the maximum amplitude modulation index, and the average optical signal power that launches into the fiber-under-test is approximately 4 dBm.

Fig. 4(a) shows a typical heterodyne electrical spectrum after coherent detection and digitizing with an intermediate frequency (IF) of about $f_{IF} \approx 3.7$ GHz. This IF needs to be higher than the chirping bandwidth to avoid spectral aliasing. Coherent homodyne detection based on an in-phase/quadrature (I/Q) receiver can also be used with a 90° optical hybrid coupler to separate the I and the Q components of the optical field and to avoid spectral aliasing. The chirped optical spectrum is then shifted from IF to the baseband in digital processing. In this process, a narrowband digital filter with 10 MHz bandwidth is used to select the IF carrier component $E_{IF}(t) = E_0(t) \exp[2\pi f_{IF}t + \varphi_n(t)]$, where $E_0(t)$ represents the low-frequency intensity noise, and $\varphi_n(t)$ represents the relative phase noise between the signal optical carrier and the

optical local oscillator. Dividing the heterodyne signal with the narrowband-filtered IF carrier in time domain shifts the IF spectrum down to the baseband, and low-frequency intensity noise and phase noise can also be minimized. The spectrum of frequency down-shifted baseband signal $E_{BB}(t) = E_{het}(t)/E_{IF}(t)$ is shown in Fig. 4(b). In addition to relatively smooth ripples in the spectrum caused by transmitter (Tx) and receiver (Rx) transfer functions, the unique feature of electrostriction induced frequency-dependent loss/gain shown as discrete spectral lines is quite weak.

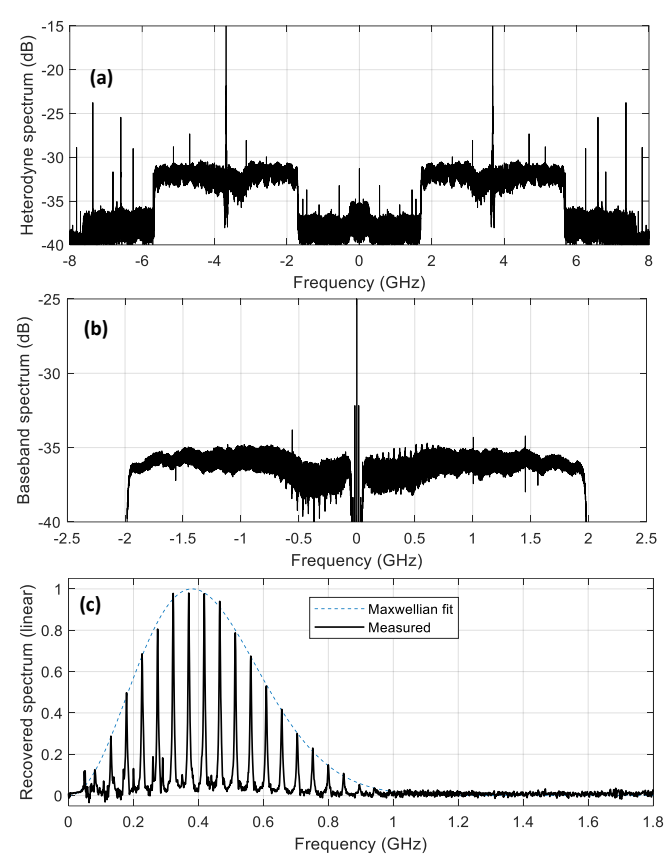


Figure 4. (a) Heterodyne IF spectrum after coherent detection, (b) Spectrum after frequency down-conversion, (c) measured electrostriction loss spectrum after digital processing.

Because the electrostriction induced frequency-dependent loss/gain spectrum is known to be anti-symmetrical, as shown in Fig. 1(c), subtraction between the spectrum of frequency down-shifted baseband signal, $\tilde{E}_{BB}(f)$, and its complex conjugate, $\tilde{E}^*_{BB}(f)$, can double the signal amplitude. In addition, as the intensity noise introduced by the system has a predominately symmetrical spectrum, this subtraction can help reduce the impact of receiver noise and improve the SNR. The SNR can also be improved by increasing the length of the waveform, increasing the number of averages, and increasing the signal optical power. Fig. 4(c) shows the resulted electrostriction loss spectrum on the positive-frequency side after subtracting between $\tilde{E}_{BB}(f)$ and $\tilde{E}^*_{BB}(f)$, correcting the deterministic Tx/Rx transfer functions, and smoothing out the spectrum by a moving average.

We have measured 5 different types of fibers using the technique discussed above, including: OFS TeraWave® fiber (G.654.E), Corning SMF-28® fiber (G.652.D), OFS

TrueWave-RS® fiber (G.655) with zero-dispersion wavelength $\lambda_0=1460nm$, Corning LEAF® fiber with $\lambda_0=1500nm$, and OFS HSDK® dispersion compensating fiber [13]. Fig. 5 shows the measured results and comparison with the loss spectrum calculated from Eq. (1), as well as Maxwellian fitting with the optimum q-value for each fiber type. Table I shows measured mode field radius r_{core} , cladding radius r_{clad} , optimum q-value, and mode field radius specified by available product specifications for the 5 fiber types.

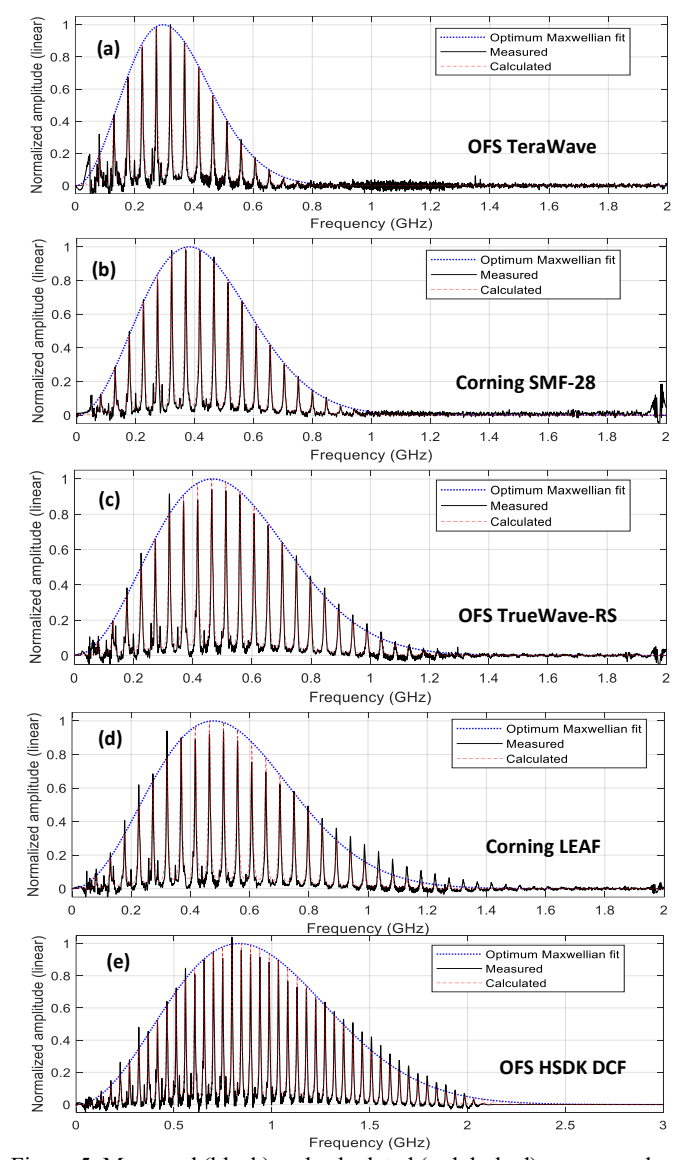


Figure 5. Measured (black) and calculated (red dashed) resonance loss spectra induced by electrostriction for 5 different fiber types, and the optimum Maxwellian fitting (blue dotted) for the spectral envelope of each fiber type.

Based on the general definition, the effective core area of a single mode fiber A_{eff} is determined by the mode field distribution E(r) as,

$$A_{eff} = \frac{2\pi \left(\int_0^\infty E(r)^2 r dr\right)^2}{\int_0^\infty E(r)^4 r dr}$$
 (9)

In many cases the mode field distribution of a single mode fiber has a Gaussian profile as described by Eq. (6), so that Eq. (9) can be simplified to $A_{eff} = \pi a^2$. Thus, the A_{eff} of the 5

fiber types described here are approximately $78 \, \mu m^2$ for SMF-28 fiber, $51 \, \mu m^2$ for TrueWave-RS fiber, $51 \, \mu m^2$ for LEAF fiber, $17 \, \mu m^2$ for DCF, and $129 \, \mu m^2$ for TeraWave fiber. Generally, with a decrease of A_{eff} , the envelope of electrostriction induced loss spectrum spreads wider, and the optimum q-value increases accordingly for the Maxwellian fitting. For the measurement of DCF which has a very small core area, 3 GHz chirping bandwidth was used in the experiment as the resonance loss spectrum of electrostriction extends beyond 2 GHz.

Fiber type	r _{core} (μm)	r _{clad} (μm)	q (MHz)	Product spec. r_{core} (µm)
SMF-28	4.99	62.4	269	5.2 ± 0.25
TrueWave-RS	4.03	62.55	334	4.2 ± 0.3
LEAF	4.04	62.55	333	4.8 ± 0.3
DCF	2.29	62.68	585	2.2
TeraWave	6.43	62.55	209	6.3 ± 0.25

Table I: Measured mode field radius r_{core} , cladding radius r_{clad} , optimum q-value, and mode field radius specified by available product specifications.

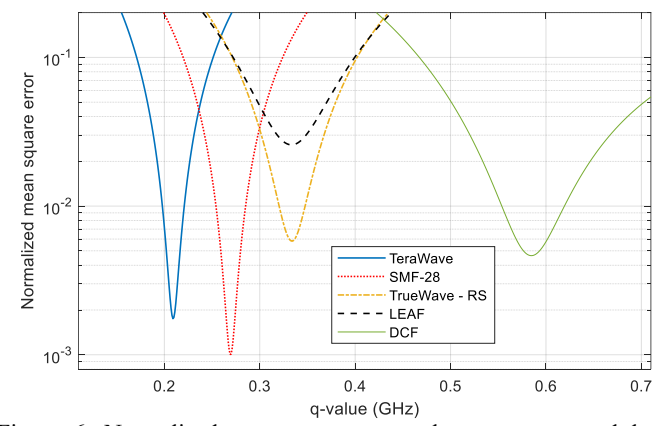


Figure 6. Normalized mean square error between measured loss spectral envelope induced by electrostriction and the Maxwellian fitting for 5 different fiber types. The optimum q-value of each fiber type can be found at the point of minimum mean square error.

Fig. 6 shows the normalized MSE as the function of q-value of Maxwellian fitting to the measured spectral envelopes of the 5 fiber types. For both TeraWave and SMF-28, the measured spectral envelopes of electrostriction fit quite well to the Maxwellian distributions with the normalized MSE close to 10^{-3} . For the other three fiber types, Maxwellian fittings are less accurate. The LEAF fiber exhibits the worst accuracy of Maxwellian fitting because the resonance loss spectrum has a longer tail than the Maxwellian distribution with the optimum q-value as can be seen in Fig. 5(d). It is well-known that LEAF fiber has an effective area larger than that of a TrueWave-RS fiber, that is inconsistent with our A_{eff} estimation through the optimum q-value of Maxwellian fitting.

Note that in all the analysis so far, we have assumed Gaussian profile for the mode field distribution as shown in Eq. (6). This approximation is valid for many step-index fibers, such as the most often used SMF-28 and its later versions such as SMF-28e, but is less accurate for fibers with tailored RIP, such as the LEAF fiber. The major reason that a LEAF (large effective area

fiber) has a larger effective area A_{eff} than a TrueWave-RS fiber is that more optical field components been extended into the cladding area [7-8], and this has been done through the modification of the RIP. We speculate that the non-Gaussian field distribution of LEAF fiber is responsible for the inaccuracy of Maxwellian fitting and the error in the A_{eff} estimation through the optimum q-value. While Gaussian mode field profile approximation helped simplifying mathematical expressions such as to obtain Eq. (7), numerical analysis will have to be used in Eqs. (1) – (5) if the mode field does not have a simple Gaussian profile. Through trial-and error, a reasonably good fit to the measured electrostriction spectrum of LEAF fiber can be obtained by using a non-Gaussian mode field profile as shown in the inset of Fig. 7, which is created from,

$$E^{2}(r) = \left\{ 3.4 \exp\left(\frac{-r^{2}}{2.23^{2}}\right) + \exp\left(\frac{-r^{2}}{2.9^{2}}\right) + 0.13 \left[\exp\left(\frac{-r^{2}}{2.9^{2}}\right) \right]^{\frac{1}{4}} \right\} / 4.53$$

which corresponds to an effective core area of approximately $65 \mu m^2$ according to Eq. (9). In the numerical process, the E(r) profile is numerically produced and used in Eqs. (2-3) to calculate the time domain electrostriction response using Eq. (1). By setting $R = \infty$ to remove multiple reflection from the circumference of the cladding, and performing Fourier transform, the envelope of electrostriction loss spectrum can be obtained, which is shown as the solid line in Fig.7. The normalized MSE in comparison to the measured spectrum is reduced to 0.0035, which is almost an order or magnitude lower than the minimum MSE of optimum Maxwellian fitting shown as dotted line in Fig.7.

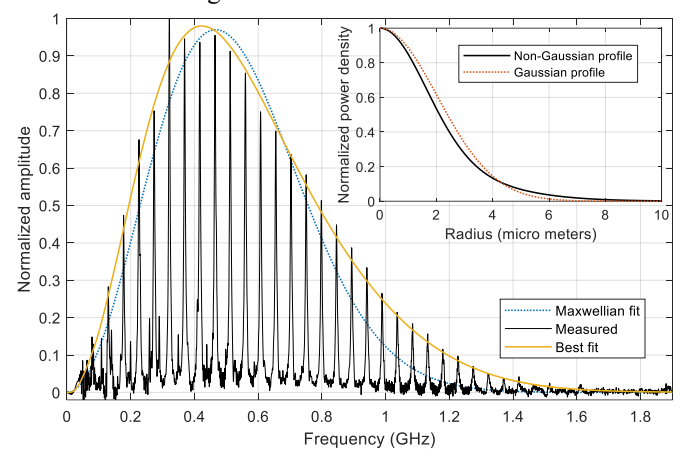


Figure 7. Measured resonance loss spectrum of LEAF fiber (black-solid). Electrostriction loss spectral envelope with optimum Maxwellian fitting (blue-dotted) and calculated with non-Gaussian field profile (yellow-solid). Inset: Gaussian (dotted) and non-Gaussian (solid) field profiles used for calculation.

In addition to the change of mode field distribution, RIP tailoring may also alter the mechanical properties of the material, such as soundwave velocity, which warrants future investigation. For example, a nanoengineered ring [14] or a fluorine-doped lower index trench [15-17] outside the core of a G.657 bend-insensitive fiber, which might contain glass with different sound transmission properties, could introduce a pair of boundaries, concentric with the outer cladding. These might alter the electrostriction spectrum by adding minor resonances at the reciprocal of the round-trip time between the core and the new interfaces. It also might change the core to cladding round

trip time to alter frequencies of associated resonances. Under these circumstances, per Eq. 7, no measurable change to the envelope of the core-cladding resonances is expected.

Throughout this investigation, we did not attempt to find the actual mode field profile E(r), instead, our purpose is to show that Gaussian mode field profile is a prerequisite for accurate Maxwellian fitting for the envelope of the electrostriction induced loss spectrum. In Fig. 6, although the optimum q-values for the TrueWave-RS and LEAF fibers are almost identical, the minimum MSE for the LEAF fiber is much higher because of the significant deviation of mode field profile from the Gaussian distribution. The normalized MSE value can be used to further improve distinguishability of fiber types. For example, we may define a modified q-value as,

$$q_n = q \cdot \left[1 - A \cdot \left(MSE_{dB,0} - MSE_{dB}\right) / MSE_{dB,0}\right]$$

where $MSE_{dB} = -10log[\min(MSE)]$, and $MSE_{dB,0} = 30$ is a constant that we set equal to MSE_{dB} measured for fibers with Gaussian mode field distribution (SMF-28 in this case) which is primarily determined by the measurement accuracy. A = 0.26 is a scaling factor chosen to make $q_n = 292 \, MHz$ for LEAF fiber, i.e. a q-value for a fiber with Gaussian mode field profile and $A_{eff} = 65 \, \mu m^2$.

Fiber type	q(MHz)	$MSE_{dB}(dB)$	$q_n(MHz)$
SMF-28 (G.652D)	269 ± 1	30 ± 0.5	269 ± 1
TW-RS (G.655)	334 ± 1	22.4 ± 0.7	312 ± 2
LEAF (G.655)	333 ± 2	15.9 ± 0.2	292 ± 0.5
DCF (HSDK [13])	585 ± 1	23.3 ± 0.4	551 ± 2
TeraWave (G.654E)	209 ± 2	27.7 ± 2	204 ± 3

Table II: electrostriction envelope parameters for five fiber types

Table II lists $[q, MSE_{dB}, q_n]$ of the five measured fiber types shown in Fig. 6, where the errors were estimated from three consecutive measurements of each fiber type [11]. It can be seen that the fiber types are more distinguishable by means of their q_n values than by sole means of their q values. Note that although the assumption of non-Gaussian field profile shown in the inset of Fig.7 produces better fit between calculated and measured envelopes of electrostriction loss spectra, the corresponding effective core area of approximately 65 μm^2 is still smaller than the product specification of about 72 μm^2 . This remains an unanswered question requiring further investigation.

In practice, there are only finite fiber types in an optical network. A database of mode field profiles of various fiber types will be useful, which can be used as possible targets for fiber type identification.

Our measurements were performed at room temperature. All the fibers used are coated fibers on spools, of 39 km for the TeraWave fiber, and 25 km for all other fibers. In practical optical networks, installed fiber cables may subject to environmental conditions such as temperature change, bending, and stress/strain, which may modify the acoustic wave through the change of geometry and mechanical properties of the fiber. For silica material, the temperature induced expansion is on the order of $5 \times 10^{-7}/C^{\circ}$ and fractional sound velocity change is about $10^{-4}/C^{\circ}$, and the elastic Young's modulus is on the order

of 7.66 ± 7.2 GPa. The first two of these will engender a reduction by ~5 kHz/C° of the core-cladding resonant frequencies. A fiber bend causes glass compression on the inner radius and glass rarefaction on the outer radius of the bend. Radial sound velocities will decrease and increase, respectively, thereby shifting the focus of a radial resonance radially toward the inner radius of the fiber bend. Core-cladding electrostriction resonances are unchanged, but the strength of the resonant absorption will decrease due to an offset between the resonance focus and the optical mode. For a 1 cm bend radius on a 125 μ m cladding diameter fiber, the size of the shift of focus is estimated to be ~0.1 μ m causing negligeable decrease of absorption. Thus, fiber bend and temperature changes are not considered significant at the 1% level of measurement error demonstrated in Table II.

In optical network applications, the electrostriction response measurement can be accomplished by a pair of digital coherent transceivers [18]. The linearly chirped waveform can be digitally created and imposed on the coherent transmitter to translate into an optical intensity modulation. The coherent optical receiver at the opposite side of the fiber converts the complex optical field into electronic domain and digitizes for signal processing based on the process described in this paper. Because electrostriction response for most fibers is limited to < 2 GHz bandwidth, as shown in Fig. 5, low speed transceivers can be used, and measurement may also be performed in the service channels of an optical network. To achieve the accuracy demonstrated in this paper, the measurement time on the order of 400 μ s (8 frames of 50 μ s waveform) is required, and more averaging can further improve the SNR.

IV. CONCLUSION

We have demonstrated a novel technique, based on an intensity-modulated single optical carrier, to characterize fiber properties by means of measuring the envelope of electrostriction induced loss spectrum. By taking advantage of anti-symmetry of the spectral envelope of electrostriction induced propagation loss, the SNR can be significantly increased by subtracting the measured spectrum from its complex conjugate. We have demonstrated that for fibers with Gaussian mode field profile, the envelope of the electrostriction-induced loss spectrum closely follows a Maxwellian distribution. Thus, the mode field radius of the fiber can be uniquely represented by a single parameter q of the best Maxwellian fitting. We have also demonstrated that for fibers with non-Gaussian mode field distribution, such as for the LEAF fiber, a radial field profile can be estimated by fitting to the measured envelope of the electrostriction-induced loss spectrum. This can potentially provide an additional mechanism for fiber type identification. We have shown that fiber type distinguishability can be improved by means of a modified q, namely q_n that takes account of the non-Gaussian nature of the radial electric field.

REFERENCES

 Y. Aoki, K. Tajima and I. Mito, "Input power limits of single-mode optical fibers due to stimulated Brillouin scattering in optical communication systems," J. Lightwave Technol., Vol. 6, pp. 710-719, 1988

- [2] E. M. Dianov, A. V. Luchnikov, A. N. Pilipetskii, A. N. Starodumov, "Long-range interaction of soliton pulse trains in a single mode fiber," Sov. Lightwave Commun., Vol. 1, pp. 37-43, 1991
- [3] E. M. Dianov, A. V. Luchnikov, A. N. Pilipetskii, and A. M. Prokhorov, Long-Range Interaction of Picosecond Solitons Through Excitation of Acoustic Waves in Optical Fibers," Appl. Phys. B, Vol. 54, pp. 175-180, 1902
- [4] A. Melloni, M. Martinelli, A. Fellegara, "Frequency Characterization of the Nonlinear Refractive Index in Optical Fiber," Fiber and Integrated Optics, Vol. 18, pp. 1-13, 1999
- [5] E. L. Buckland and R. W. Boyd, "Measurement of the frequency response of the electrostrictive nonlinearity in optical fibers," Opt. Lett., Vol. 22, pp. 676-678, 1997
- [6] R. Hui, C. Laperle, M. Reimer, A. D. Shiner, and M. O'Sullivan, "Characterization of Electrostriction Nonlinearity in a Standard Single-Mode Fiber Based on Coherent Detection and Cross-Phase Modulation," J. Lightwave Technol., vol. 33, 2015.
- [7] Y. Liu, A. J. Antos and M. A. Newhouse, "Large effective area dispersionshifted fibers with dual-ring index profiles," paper WK15, Optical Fiber Communications, OFC, San Jose, CA, USA, 1996.
- [8] Katsunari Okamoto, Fundamentals of Optical Waveguides (Optics & Photonics Series) 2nd Edition, Academic Press 2005. Section: 3.10.2 Dispersion-shifted Fibers.
- [9] R. Hui and M. O'Sullivan, Fiber-optic measurement techniques, 2nd edition (Chapter 7 Measurement errors), Academic Press, 2022.
- [10] C. C. Lee and S. Chi, "Measurement of stimulated-Brillouin-scattering threshold for various types of fibers using Brillouin optical-time-domain reflectometer," IEEE Photonics Technol. Lett., Vol. 12, pp. 672-674, 2000.
- [11] F. Al-Shaikhli, M. O'Sullivan, and R. Hui, "Direct Electrostriction Measurement using SPM for Fiber Type Identification," paper W4C.2, Optical Fiber Communications, OFC, San Diego, CA, USA, 2023.
- [12] E. M. Dianov, A. V. Luchnikov, A. N. Pilipetskii, and A. N. Starodumov, "Electrostriction mechanism of soliton interaction in optical fibers," Opt. Lett., Vol.15, pp. 314-316, 1990.
- [13] L. Gruner-Nielsen et al., "Dispersion-compensating fibers," J. Lightwave Technol., Vol. 23, pp. 3566-3579, 2005.
- [14] M-J. Li et al., "Ultra-Low Bending Loss Single-Mode Fiber for FTTH," J. Lightwave Technol., Vol. 27, pp. 376-382, 2009
- [15] K. Himeno, S. Matsuo, N. Guan and A. Wada, "Low-bending-loss single-mode fibers for fiber-to-the-home," J. Lightwave Technol., Vol. 23, pp. 3494-3499, 2005.
- [16] L. de Montmorillon, et al, "All-Solid G.652.D Fiber with Ultra Low Bend Losses Down to 5 mm Bend Radius," paper OTuL3, Optical Fiber Communication Conference/National Fiber Optic Engineers Conference, OFC/NFOEC, San Diego, CA, 2009
- [17] D. Peckham, "Bend Insensitive, Single Mode Fiber Design Strategies," paper NTuC3, Optical Fiber Communication Conference/National Fiber Optic Engineers Conference, OFC/NFOEC, San Diego, CA, 2008.
- [18] R. Hui, C. Laperle and M. O'Sullivan, "Measurement of Total and Longitudinal Nonlinear Phase Shift as Well as Longitudinal Dispersion for a Fiber-Optic Link Using a Digital Coherent Transceiver," J. Lightwave Technol., Vol. 40, pp. 7020-7029, 2022.